Article

Cooperative Hydrogen-Bonding Effects in a Water Square: A Single-Crystal Neutron and Partial Atomic Charges and Hardness Analysis Study

David R. Turner, Marc Henry, Clive Wilkinson, Garry J. McIntyre,
Sax A. Mason, Andres E. Goeta, and Jonathan W. Steed

J. Am. Chem. Soc., **2005**, 127 (31), 11063-11074• DOI: 10.1021/ja052081a • Publication Date (Web): 16 July 2005

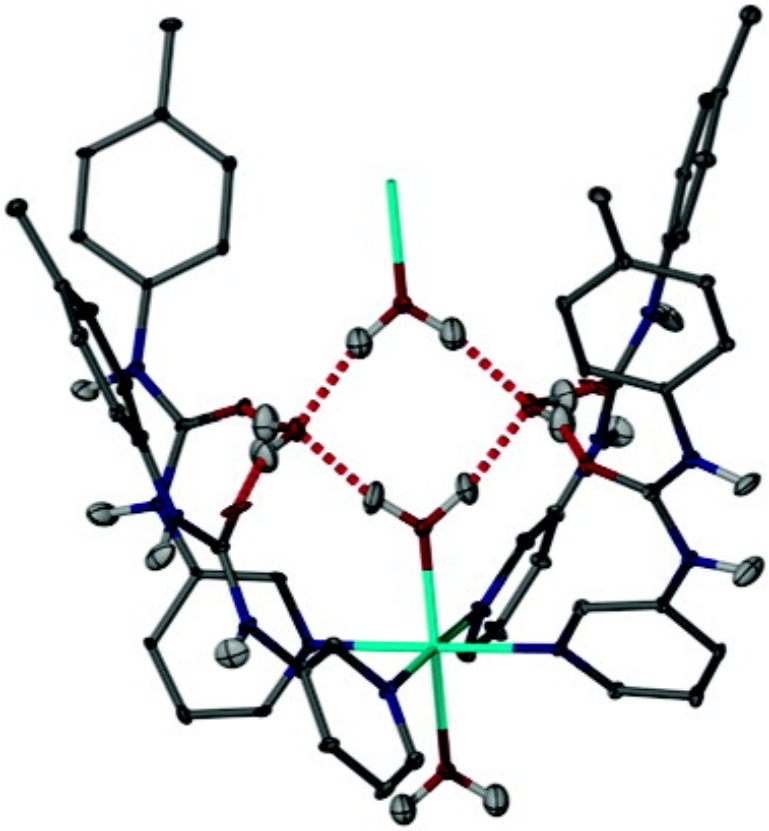

J|A|C|S
ARTICLES
Published on Web 07/16/2005

Cooperative Hydrogen-Bonding Effects in a Water Square: A Single-Crystal Neutron and Partial Atomic Charges and Hardness Analysis Study

David R. Turner,[†] Marc Henry,[‡] Clive Wilkinson,[†] Garry J. McIntyre,[§] Sax A. Mason,[§] Andres E. Goeta,[†] and Jonathan W. Steed*,[†]

Contribution from the Department of Chemistry, University of Durham, South Road, Durham DH1 3LE, U.K., Institut Le Bel, Universite Louis Pasteur, 4, Rue Blaise Pascal, 67070 Strasbourg Cedex, France, and Institut Laue-Langevin, B.P. 156, 38042 Grenoble Cedex 9, France

Received April 1, 2005; E-mail: jon.steed@durham.ac.uk

Abstract: Four isomorphous complexes of formula $[M(L)_4(H_2O)_2]SO_4 \cdot 2H_2O$ (M = Co, **1a**; Ni, **1b**; Cu, **1c**; Zn, **1d**) have been isolated and characterized by single-crystal X-ray diffraction and neutron diffraction using the quasi-Laue diffractometer VIVALDI at the Institut Laue-Langevin as well as by thermogravimetric analysis. The structures contain a discrete, strongly hydrogen-bonded water tetramer which causes a significant distortion of the metal coordination sphere in each case. Partial atomic charges and hardness analysis (PACHA) calculations reveal that the shortest hydrogen bonds are not the strongest in this constrained, cyclic solid-state structure and show that the distortion at the metal center is caused by the drive to maintain the integrity of the water tetramer. The system undergoes a disorder−order transition on slow cooling that provides insight into the nature of communication between water squares.

Introduction

The solid-state chemistry of water clusters continues to attract considerable attention.[1−10] It seems clear that trapping small, finite "icicles" within a crystalline host matrix offers considerable scope for isolating and studying their properties, some of which may be of relevance to biological systems[11−17] or clathrate hydrate research.[18−20] The observation of small water aggregates of a variety of structural types within organic or metal−organic crystal structures is commonplace. For example, a search of the Cambridge Structural Database (CSD)[21] for structures containing at least three ordered water molecules, with H atoms located and O−H bond distances normalized to typical neutron values, mutually linked with H···O contacts within the sum of the van der Waals radii, reveals a total of 2267 hits. Thus, the mere occurrence of water clusters per se is not cause for comment. However, the detailed study of isolated water cluster inclusion compounds can shed considerable light on the properties of extended networks and the way in which water, as a ubiquitous solvent, influences its surroundings. There is also particular interest in local ordering in liquid water as a means of rationalizing its anomalous physical properties.[22,23] The study of water aggregates by X-ray crystallography has received a significant boost with the advent of high-precision, low-temperature crystallographic methods, particularly in the ability to locate hydrogen atom electron density.[24] However, single-crystal neutron diffraction remains the tool of choice for experimental location of hydrogen atom positions,[25] particularly for input into theoretical calculations such as PACHA (Partial

[†] University of Durham.
[‡] Universite Louis Pasteur.
[§] Institut Laue-Langevin.

(1) Ghosh, S. K.; Bharadwaj, P. K. *Angew. Chem., Int. Ed.* **2004**, *43*, 3577−3580.
(2) Barbour, L. J.; Orr, G. W.; Atwood, J. L. *Nature* **1998**, *393*, 671−673.
(3) Barbour, L. J.; Orr, G. W.; Atwood, J. L. *Chem. Commun* **2000**, 859−860.
(4) Ghosh, S. K.; Bharadwaj, P. K. *Inorg. Chem.* **2004**, *43*, 6887−6889.
(5) Henry, M. *ChemPhysChem* **2002**, *3*, 607−616.
(6) Infantes, L.; Motherwell, S. *Cryst. Eng. Commun.* **2002**, *4*, 454−461.
(7) Muller, A.; Henry, M. *C. R. Chim.* **2003**, *6*, 1201−1208.
(8) Steiner, T.; Saenger, W. *Acta Crystallogr. Sect. D−Biol. Crystallogr.* **1993**, *49*, 592−593.
(9) Wang, L. S.; Wang, R. S. *Prog. Chem.* **2001**, *13*, 81−86.
(10) Yoshizawa, M.; Kusukawa, T.; Kawano, M.; Ohhara, T.; Tanaka, I.; Kurihara, K.; Niimura, N.; Fujita, M. *J. Am. Chem. Soc.* **2005**, *127*, 2798−2799.
(11) Smith, J. C.; Merzel, F.; Bondar, A. N.; Tournier, A.; Fischer, S. *Philos. Trans. R. Soc. London Ser. B−Biol. Sci.* **2004**, *359*, 1181−1189.
(12) Bogacheva, E. N.; Gedrovich, A. V.; Shishkov, A. V. *Colloid J.* **2004**, *66*, 137−140.
(13) Ceruso, M.; Weinstein, H. *Biophys. J.* **2004**, *86*, 266A−266A.
(14) Papoian, G. A.; Ulander, J.; Eastwood, M. P.; Luthey-Schulten, Z.; Wolynes, P. G. *Proc. Natl. Acad. Sci. U.S.A.* **2004**, *101*, 3352−3357.
(15) Batchelor, J. D.; Olteanu, A.; Tripathy, A.; Pielak, G. J. *J. Am. Chem. Soc.* **2004**, *126*, 1958−1961.
(16) Garcia-Sosa, A. T.; Mancera, R. L.; Dean, P. M. *J. Mol. Model.* **2003**, *9*, 172−182.
(17) Smith, J. C.; Merzel, F.; Verma, C. S.; Fischer, S. *J. Mol. Liq.* **2002**, *101*, 27−33.
(18) Udachin, K. A.; Ripmeester, J. A. *Nature* **1999**, *397*, 420−423.
(19) Udachin, K. A.; Ratcliffe, C. I.; Ripmeester, J. A. *Angew. Chem., Int. Ed.* **2001**, *40*, 1303−1305.
(20) Ripmeester, J. A. Hydrate research−From correlations to a knowledge-based discipline−The importance of structure. In *Gas Hydrates: Challenges for the Future*; Holder, G. D., Bishnoi, P. R., Eds.; New York Academy of Sciences: New York, 2000; Vol. 912, pp 1−16.
(21) CSD, Version 5.25, Nov 2003 + 1 update (Jan 2004).
(22) Benson, S. W.; Siebert, E. D. *J. Am. Chem. Soc.* **1992**, *114*, 4269−4276.
(23) Day, M. B.; Kirschner, K. N.; Shields, G. C. *Int. J. Quantum Chem.* **2005**, *102*, 565−572.
(24) Howard, J. A. K.; Copley, R. C. B.; Goeta, A. E.; Lehmann, C. W.; Cole, J. C.; Yufit, D. S.; Archer, J. R. *J. Appl. Crystallogr.* **1997**, *30*, 413.
(25) Bouquiere, J. P.; Finney, J. L.; Lehmann, M. S.; Lindley, P. F.; Savage, H. F. J. *Acta Crystallogr., Sect. B* **1993**, *49*, 79−89.

Atomic Charges and Hardness Analysis) as an aid to a full understanding of hydrogen-bonding interplay.[5,7,26]

Within water clusters such as the clathrate hydrates and in the various forms of ice itself, for example, structures involving five- and six-membered rings of water molecules are common,[20,27,28] with water pentagons forming a major part of the hydration of the protein crambin.[29] Four-membered rings are rarer (though far from unknown[30]) because of unfavorable H···H repulsions (which can be overlooked due to the difficulty in studying hydrogen bonding by X-ray methods) across the smaller ring. However, they are a key component of a novel, recently reported clathrate hydrate structure[19] and form the basis for the controversial octamer model of liquid water proposed by Benson and Siebert.[22] We now report variable-temperature single-crystal X-ray, neutron, and thermogravimetric studies of an isomorphous series of compounds $[M(L)_4(H_2O)_2]SO_4 \cdot 2H_2O$ (M = Co, **1a**; Ni, **1b**; Cu, **1c**; Zn, **1d**) of the ureidopyridyl ligand, L, in which a discrete water tetramer is held between a pair of metal ions. The neutron data have been used to analyze the structures by means of the PACHA method,[5,7,26] allowing a full understanding of the hydrogen bonding in the water tetramer itself and of its influence on its environment. Part of this work has been published in preliminary form.[31]

Results and Discussion

X-ray Structures. Ligand L binds to transition metal centers via the pyridyl nitrogen atom while simultaneously hydrogen bonding to anions via the urea functionality. While the ligand and its analogues can form anion chelate complexes of type AgL_2^+ or CoL_4^{2+} with nitrate and with solvent molecules as the guest species, transition metal complexes of L more usually form hydrogen-bonded polymers in the solid state.[32−35] Complexes of bipyridyl bis(urea) analogues of L also exhibit novel guest binding properties[33] and act as gelling agents.[36] Reaction of L with a variety of hydrated transition metal sulfate salts results in the formation of a highly insoluble, isomorphous series of discrete 4:1 complexes $[M(L)_4(H_2O)_2]SO_4 \cdot 2H_2O$ (M = Co, **1a**; Ni, **1b**; Cu, **1c**; Zn, **1d**; Scheme 1).

The structures of the four compounds of type **1** consist of infinite chains composed of repeating $[M(L)_4(H_2O)_2]^{2+}$ units (Figure 1). Within these units, the four equatorial pyridyl ligands adopt a twisted "cup-shaped" geometry, with the aqua ligands occupying the axial coordination sites. The oxygen atoms of the urea-containing ligands point toward the interior cavity. The conformation of the $[M(L)_4(H_2O)_2]^{2+}$ complex allows for a quadruple helical chain of pitch 32.48 Å to be assembled in which the individual units can stack "head-to-tail" within each other. There are edge-to-face π-stacking interactions formed

Scheme 1

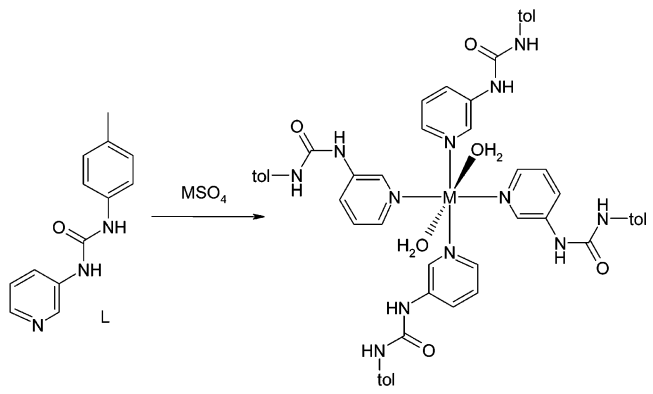

M = Co(II) **1a**, Ni(II) **1b**, Cu(II) **1c**, Zn(II) **1d**

between the tolyl rings of one complex and the pyridyl rings of the complex immediately above. The chains are primarily held together by strong hydrogen bonds from the two water molecules that are enclathrated within the intracomplex cavities (Figure 1b). Each of these guest water molecules donates hydrogen bonds to two urea oxygen atoms and receives hydrogen bonds from the aqua ligands above and below it to give a discrete water tetramer. Each enclathrated water molecule is therefore held in place by a total of four hydrogen bonds. A search of the CSD reveals a total of 32 other such metal-coordinated tetramers, although the overwhelming majority (30) are centrosymmetric. Of those 32, in only three structures are the metals and oxygen atoms coplanar as in the present case, requiring sp^2 hybridization at the coordinated water.[37−39] The distorted square water tetramer within the cavity exhibits enclathrated water molecules disordered across two positions at 120 K in space group *P*4/*n*. In principle it appears that a water octahedron comprising six water molecules could be accommodated within the cavity; however, it is clear that such a situation would result in unfavorable water···water interactions. The formulation of a total of only four water molecules in each case was confirmed by elemental analysis and thermogravimetric analysis (vide infra).

The individual chains in the structure are parallel to one another, aligned with the *c* axis (Figure 2). The chains are held together by the sulfate counteranions, which are situated on $\bar{4}$ special positions and are also aligned with the *c* axis in voids between the $[M(L)_4(H_2O)_2]^{2+}$ stacks. Each sulfate is hydrogen bonded to four separate $[M(L)_4(H_2O)_2]^{2+}$ complexes via two NH···O interactions in an $R_2^2(8)$ motif (Figure 3).[40] The average length of these interactions in the four structures (d(H···A)) is 2.14 Å (Table 1), with no apparent trend or difference between the four isomorphous materials. This leads to the sulfate anion being held in place by a total of eight interactions and therefore being hydrogen bond saturated (i.e., all of the oxygen lone pairs are involved in accepting hydrogen bonds).[41] The twisted geometry of the L ligands around the metal center appears to arise from the crystal packing, as it allows for an alignment of the urea groups with the sulfate anions forming the $R_2^2(8)$ rings and optimal π-stacking along the chain.

(26) Henry, M.; Hosseini, M. W. *New J. Chem.* **2004**, *28*, 897−906.
(27) Ball, P. *H2O: A Biography of Water*, 1st ed.; Phoenix: London, 2004.
(28) Steed, J. W.; Atwood, J. L. *Supramolecular Chemistry*, 1st ed.; J. Wiley & Sons: Chichester, 2000.
(29) Teeter, M. M. *Proc. Natl. Acad. Sci. U.S.A.* **1984**, *81*, 6014−6018.
(30) Long, L. S.; Wu, Y. R.; Huang, R. B.; Zheng, L. S. *Inorg. Chem.* **2004**, *43*, 3798−3800.
(31) Turner, D. R.; Hursthouse, M. B.; Light, A. E.; Steed, J. W. *Chem. Commun.* **2004**, 1354−1355.
(32) Turner, D. R.; Smith, B.; Spencer, E. C.; Goeta, A. E.; Evans, I. R.; Tocher, D. A.; Howard, J. A. K.; Steed, J. W. *New J. Chem.* **2005**, *29*, 90−98.
(33) Applegarth, L.; Goeta, A. E.; Steed, J. W. *Chem. Commun.* **2005**, 2405−2406.
(34) Turner, D. R.; Spencer, E. C.; Howard, J. A. K.; Tocher, D. A.; Steed, J. W. *Chem. Commun* **2004**, 1352−1353.
(35) Turner, D. R.; Smith, B.; Goeta, A. E.; Evans, I. R.; Tocher, D. A.; Howard, J. A. K.; Steed, J. W. *Cryst. Eng. Commun.* **2004**, *6*, 633−641.
(36) Applegarth, L.; Steed, J. W., unpublished work.
(37) Hay, B. P.; Hancock, R. D. *Coord. Chem. Rev.* **2000**, *212*, 61−78.
(38) Best, S. P.; Figgis, B. N.; Forsyth, J. B.; Reynolds, P. A.; Tregennapiggott, P. L. W. *Inorg. Chem.* **1995**, *34*, 4605−4610.
(39) Beattie, J. K.; Best, S. P. *Coord. Chem. Rev.* **1997**, *166*, 391−415.
(40) Etter, M. C. *Acc. Chem. Res* **1990**, *23*, 120−126.
(41) Loehlin, J. H.; Franz, K. J.; Gist, L.; Moore, R. H. *Acta Crystallogr., Sect. B* **1998**, *54*, 695−704.

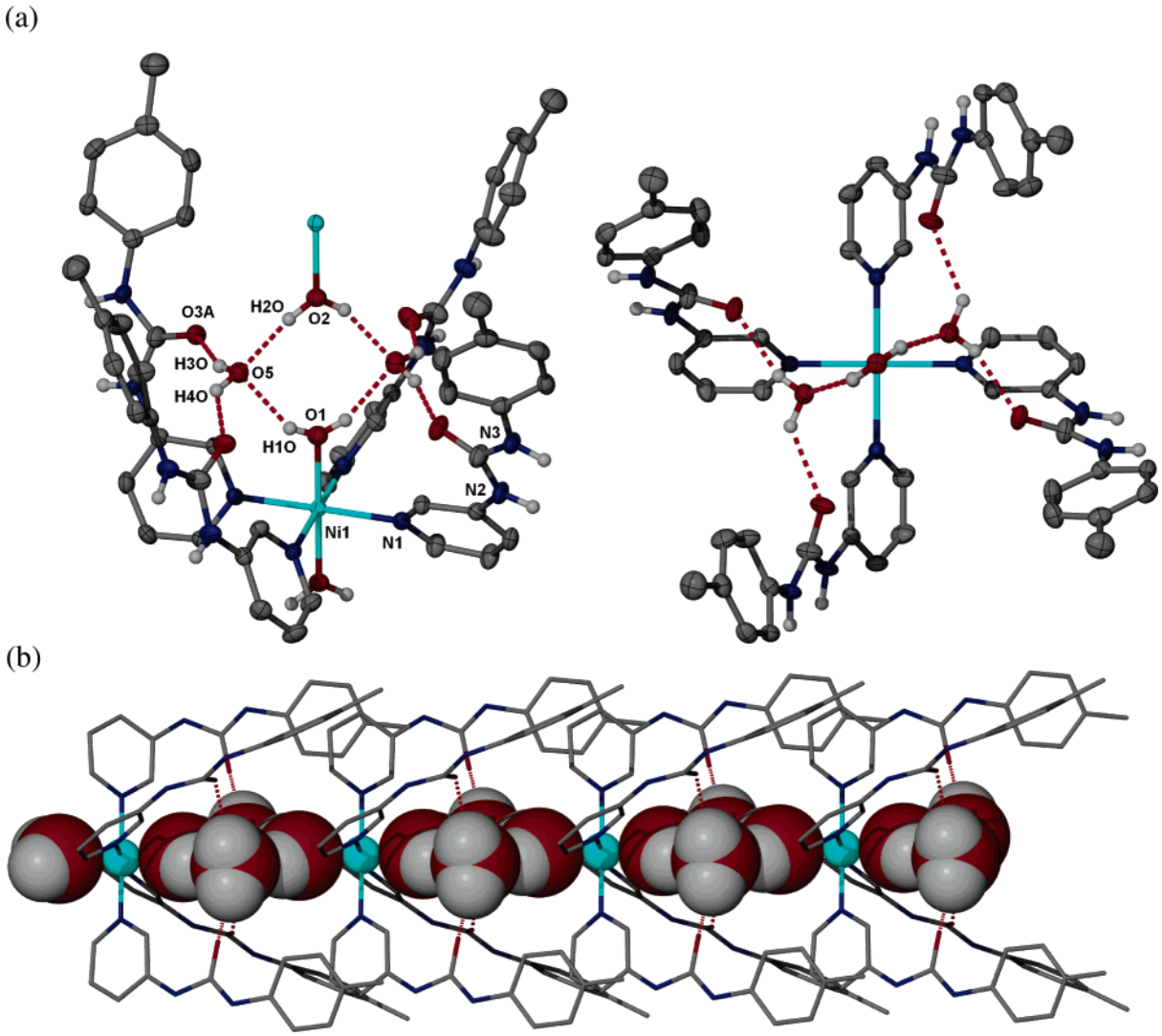

Figure 1. (a) Thermal ellipsoid plot (50%) of one repeating $[Ni(L)_4(H_2O)_2]^{2+}$ unit from the X-ray structure of **1a** at 120 K, showing the twisted arrangement of the equatorial ligands and atom-labeling scheme adopted for disordered *P*4/*n* structures. Symmetry equivalents of the Ni atom and the "lower" water molecule based on O(2) are also shown; C−H hydrogen atoms are omitted for clarity. (b) View of $[Ni(L)_4(H_2O)_2]^{2+}$ along the *c* axis. (c) A section of an infinite strand running through the structures of complexes **1**, showing the interactions between the enclathrated water molecules, the aqua ligands, and the urea oxygen atoms. Only the water hydrogen atoms are shown for clarity. The nickel(II) ions and water molecules are shown in space-filling mode.

Initially, the modeling of the X-ray data collected at 120 K proved challenging, as satisfactory solutions are obtainable using either one of the tetragonal space groups *P*4/*n* or $P\bar{4}$. The difference between these two space groups, as far as the modeling of these systems is concerned, is whether the asymmetric unit contains a quarter (*P*4/*n*) or a half ($P\bar{4}$) of one $[M(L)_4(H_2O)_2]^{2+}$ complex. In both space groups there is resolvable disorder of the urea oxygen atom and the water square across two positions (Figure 4). Using *P*4/*n*, the disordered solvent is modeled in a single position with an occupancy of 50%, giving the total of two enclathrated water molecules per formula unit. In $P\bar{4}$, the relative proportion of the two water square orientations may be refined with total occupancy set to 100%. The proportion differed between structures in the region of 20−50%, suggesting in some cases a nonrandom distribution of water tetramer orientations although, in general, occupancies were close to 50% and hence *P*4/*n* was the appropriate space group choice at this temperature. The disordered water distribution could take the form of random orientations along an individual chain (and hence no intertetramer communication) or a random distribution of individually ordered chains with 1D communication along the chain axis.

To address this question a sample of $[Co(L)_4(H_2O)_2]SO_4 \cdot 2H_2O$ crystal was placed on a diffractometer at room temperature and cooled to 30 K under an open helium flow over the course of 3 h. Data were then collected before removing the crystal. The sample was left to warm to room temperature for 15 min before being flash cooled under the helium stream, and data were re-collected. These data sets showed that the slow-cooled sample displayed a perfectly ordered structure in $P\bar{4}$ at 30 K (half the complex unique and only one set of sites, A or B in Figure 4, occupied), whereas the flash-cooled sample displayed a 45:55 occupancy of the water positions. It therefore appears that the disorder resolves itself as the sample is gradually cooled to give a lower symmetry structure. However, when the sample is rapidly cooled it does not have time to order itself and a "snapshot" of the disorder is obtained. Intermediate cooling rates result in partial ordering, giving nonrandom distribution of the enclathrated solvent. The observation of a full ordered structure in $P\bar{4}$ in the slow-cooled sample at 30 K implies communication

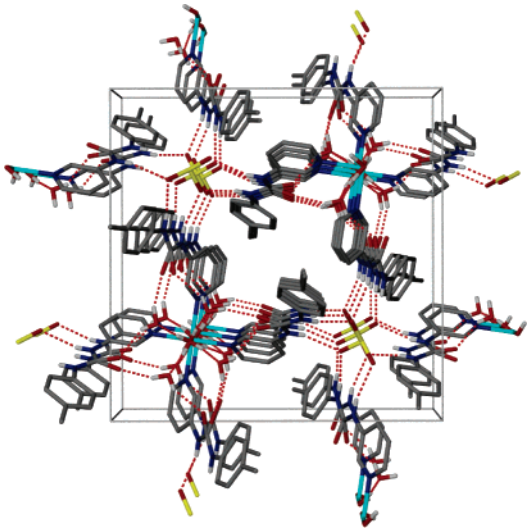

Figure 2. View of the X-ray crystal structure of the cobalt complex **1a** along the crystallographic *c* axis, showing the arrangement of the parallel $[M(L)_4(H_2O)_2]^{2+}$ strands around the sulfate counteranions. Both disordered water positions are shown. Non-interacting hydrogen atoms are omitted for clarity.

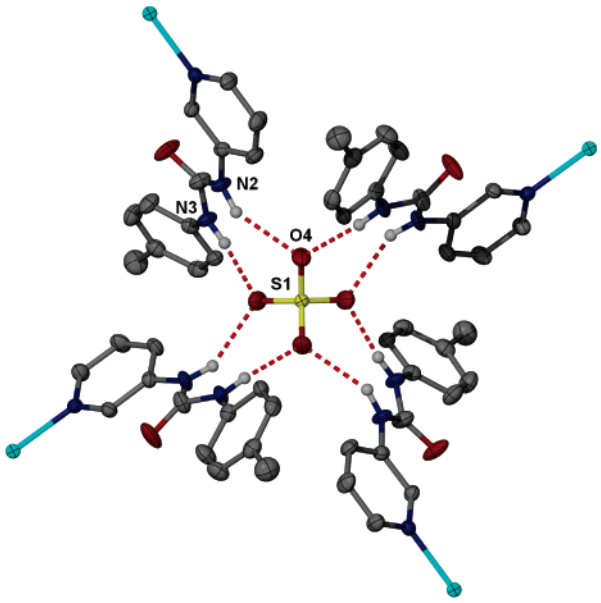

Figure 3. The sulfate anion is surrounded by four L ligands and receives a total of eight hydrogen bonds in four $R_2^2(8)$ motifs. CH hydrogen atoms are omitted for clarity. Hydrogen bond data are shown in Table 1.

both within and *between* chains, the latter presumably mediated by the strong hydrogen bonds to SO_4^{2-} which are intimately linked to the disordered urea. It is thus likely that each individual chain is ordered with significant intercavity communication, but at higher temperatures the interchain interaction energy becomes small compared to thermal energies and hence interchain order is lost.

Influence on Coordination Geometry. One of the most interesting features of this series of materials is the effect that the hydrogen bonding of the water tetramer has upon the coordination environment of the metal center. The strength of the hydrogen bonding is such that the "lower" aqua ligand, O(2), is pulled away from the metal, producing a linear distortion of the O−M−O axis (Table 2). This effect is seen for all of the metals but is especially pronounced for the Cu(II) compound,

Table 1. Hydrogen Bond Data for the NH···SO_4^- Interactions[a]

	d(D–H)/ Å	*d*(H···A)/ Å	*d*(D···A)/ Å	∠(D−H···A)/ deg
Co complex (**1a**)				
N(2)−H(2N)···O(4)	0.82(3)	2.25(3)	3.038(2)	164(3)
N(3)−H(3N)···O(4)′	0.85(3)	1.99(3)	2.834(2)	171(3)
Ni complex (**1b**)				
N(2)−H(2N)···O(4)	0.79(2)	2.29(2)	3.067(3)	168(2)
N(3)−H(3N)···O(4)′	0.78(2)	2.08(2)	2.852(3)	171(2)
Cu complex (**1c**)				
N(2)−H(2N)···O(4)	0.84(3)	2.18(3)	3.000(2)	164(2)
N(3)−H(3N)···O(4)′	0.85(3)	2.01(3)	2.843(2)	168(2)
Zn complex (**1d**)				
N(2)−H(2N)···O(4)	0.76(2)	2.30(2)	3.044(2)	166(2)
N(3)−H(3N)···O(4)′	0.84(2)	2.01(2)	2.841(2)	171(2)

[a] Primed atoms are related by $-y + 1$, $x + {}^1/_2$, $-z + 1$.

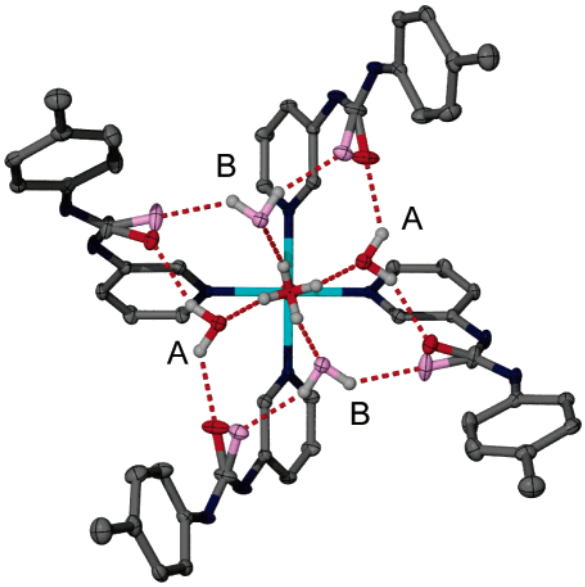

Figure 4. A $[Cu(L)_4(H_2O)_2]^{2+}$ unit, showing the two disordered positions (A, B) of the urea oxygen atoms and the enclathrated solvent in *P*4/*n* in different shades. Thermal ellipsoids are displayed at 50% probability. Hydrogen atoms (except those of water) are omitted for clarity.

Table 2. M−OH_2 Bond Lengths in the $[M(L)_4(H_2O)_2]SO_4{\cdot}2H_2O$ Structures, Highlighting the Linear Distortion of the O−M−O Axis[a]

	M–O(1)/Å	M–O(2)/Å	ΔM–O/Å
Co	2.074(3)	2.182(3)	0.055
Ni	2.077(4)	2.121(4)	0.044
Cu	2.282(3)	2.458(4)	0.176
Zn	2.126(3)	2.188(3)	0.062

[a] O(1) refers to the "upper" oxygen atom in Figure 6.

presumably due to its Jahn−Teller distortion and consequently weak axial M−OH_2 bonds. An examination of mean M−OH_2 bond lengths for each of the metals used was carried out using the CSD (Figure 5).[21,42] These searches revealed that the inequality in the M−OH_2 distances in the $[M(L)_4(H_2O)_2]SO_4{\cdot}2H_2O$ structures stems from an elongation of the M−O(2) distance rather than a situation in which the M−O(1) bond is contracted.

It is not uncommon for crystal packing effects to influence the coordination environment of a transition metal center, although such distortions most often occur in more than one dimension and are combined with a deformation of the

(42) Allen, F. H. *Acta Crystallogr., Sect. B* **2002**, *58*, 380−388.

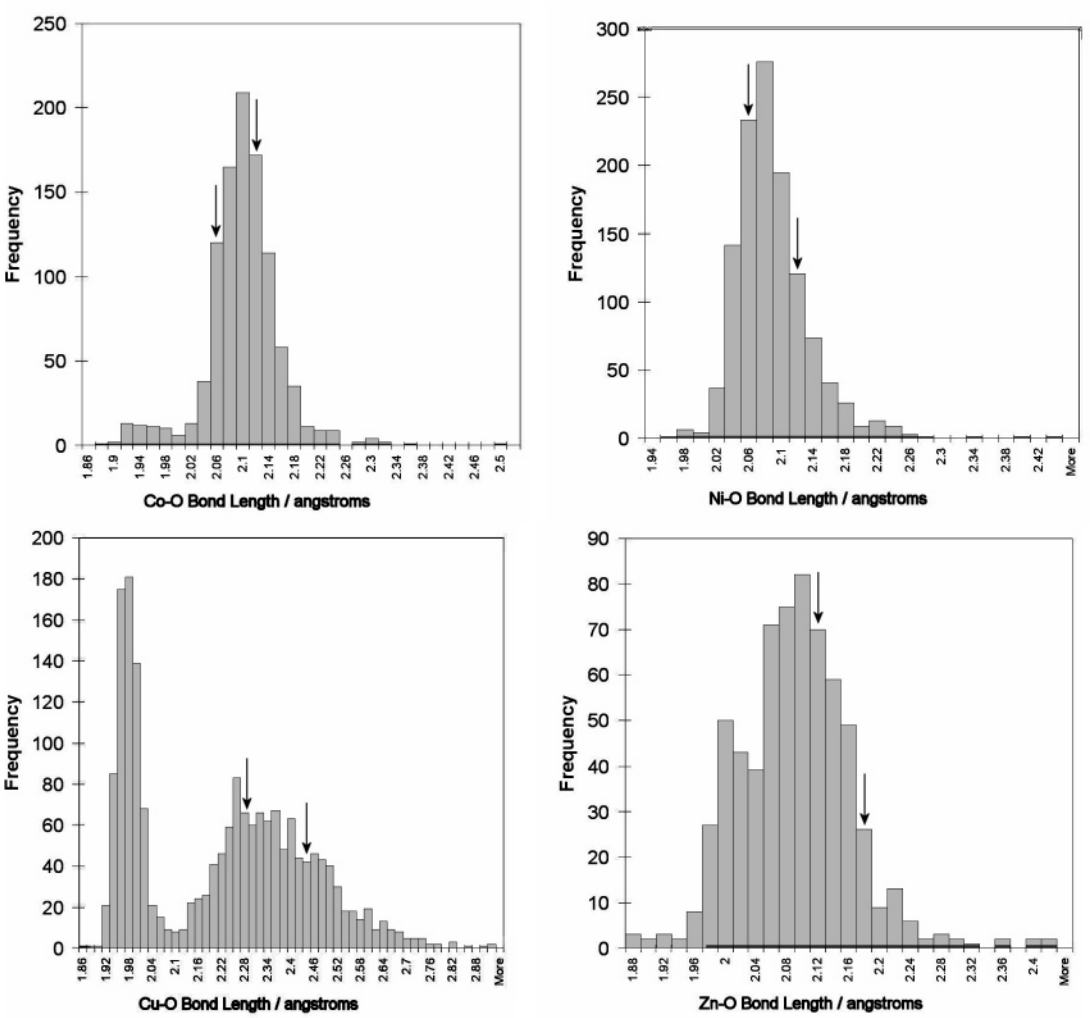

Figure 5. Results of the CSD search examining average M−OH_2 distances for the metals (Co, Ni, Zn, and Cu, clockwise from top left) in the $[M(L)_4(H_2O)_2]SO_4 \cdot 2H_2O$ complexes. Results from this work are indicated by arrows showing that, in all cases, one of the bonds is toward the higher end of the ranges, i.e., stretched by hydrogen bonding in the water tetramer.

octahedral angles around the metal. The CSD was used to search for other transition metal compounds with *trans*-aqua ligands to examine the occurrence of structures that are similarly distorted in only one dimension. Search criteria were used in which the octahedral angles around the transition metal were restricted to $90 \pm x°$, with a variation in x allowing for searches to be conducted in which the closeness of the metal center to an exact octahedral geometry can be assessed. When restricted to an angular deviation of within one degree, no structures were found to have a distortion of the O−M−O axis (i.e., all compounds had identical M−OH_2 distances). This makes the $[M(L)_4(H_2O)_2]SO_4 \cdot 2H_2O$ complexes unique in the extent of the length distortion while maintaining a rigid octahedral geometry around the metal center. When the search criteria were relaxed to within two degrees, some structures were found that do display a linear distortion, although the vast majority of structures displayed equal bond lengths (Figure 6). The structures that were found to show the most pronounced asymmetry of the O−M−O axis, apart from those in this work, were three Cu(II)-containing complexes, in which the aqua ligands are influenced by interactions with neighboring molecules,[43−45] and a Co(II)/Cu(II) compound reported by Atwood et al.[2,3] This latter structure is particularly interesting, as enclathrated water is responsible for drawing one of the aqua ligands away from the metal center in an manner analogous to that observed for the $[M(L)_4(H_2O)_2]SO_4 \cdot 2H_2O$ complexes. There were no examples of distorted nickel or zinc compounds found within the $x = 2°$ tolerance range. When the search criteria were relaxed to allow angles of $90 \pm 3°$, more structures were found to display distorted axes, although this is obviously coupled with the distortion of the coordination geometry around the metal center. Aqua ligands on lanthanides have also been shown to exhibit linear distortions upon interaction with enclathrated water, with key consequences for the understanding of water exchange in the application of such complexes as MRI contrast agents.[46]

The enclathrated water molecules within the $[M(L)_4(H_2O)_2]SO_4 \cdot 2H_2O$ series clearly have an influence on the metal center. Such an effect must arise from the strength of the hydrogen-bonding interactions in which the four water molecules engage.

(43) Naumov, P.; Ristova, M.; Soptrajanov, B.; Drew, M. G. B.; Ng, S. W. *Croat. Chem. Acta* **2002**, *75*, 701−711.

(44) Filippova, I. G.; Kravtsov, V. K.; Gdanec, M. *Russ. J. Coord. Chem.* **2000**, *26*, 809−816.

(45) Chattopadhyay, D.; Chattopadhyay, S. K.; Lowe, P. R.; Schwalbe, C. H.; Mazumder, S. K.; Rana, A.; Ghosh, S. *J. Chem. Soc., Dalton Trans.* **1993**, 913−916.

(46) Parker, D.; Dickins, R. S.; Puschmann, H.; Crossland, C.; Howard, J. A. K. *Chem. Rev.* **2002**, *102*, 1977−2010.

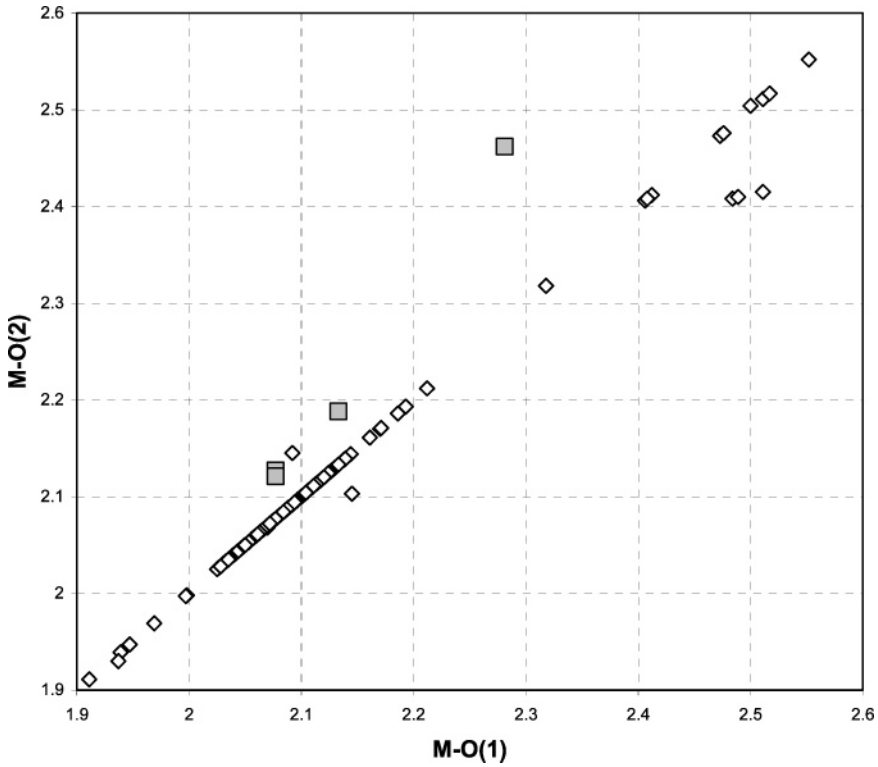

Figure 6. Results of a CSD search of *trans*-diaqua structures for M = Co, Ni, Cu, and Zn within the tolerance range 90 ± 2° around the octahedral center, showing that most structures display equal M−O lengths. Results from this work are displayed as squares.

X-ray crystallographic data provide only limited information about hydrogen bond parameters due to the low electron density of hydrogen atoms and systematic shortening of the D−H bond length.[47] Neutron diffraction data are able to provide much better information and more accurate hydrogen positions, as they rely upon diffraction from nuclei rather than electron density. Crystals of a suitable size for neutron diffraction were obtained for the Co, Ni, and Zn complexes (although not Cu despite repeated attempts) and were subjected to single-crystal neutron analysis.

Neutron Diffraction. Neutron diffraction studies on the Co, Ni, and Zn complexes (**1a**, **1b**, and **1d**) were carried out at the Institut Laue-Langevin, Grenoble, using the diffractometer VIVALDI (VIVALDI = Very Intense Vertical Axis Laue Diffractometer) with thermal neutron radiation (λ = 0.8−5.0 Å).[48] The VIVALDI instrument uses a drum detector to collect diffraction data over a solid angle of 8 steradian, and is especially suitable for small-molecule samples (primitive unit cells with cell lengths less than 25 Å). The sample is housed within a cryostat, allowing data collection temperatures as low as 1.5 K to be reached routinely. The reasons for our use of this instrument, as opposed to a conventional monochromatic diffractometer, are the rapid experiment times (ca. 8 h instead of one week) and the ability to use relatively small crystals.[49] As a result, we were able to collect full single-crystal neutron diffraction data at two or three temperatures on three samples of modest-sized crystals within a period of a few days. For reference, room-temperature data on the zinc complex **1d** were collected on the monochromatic instrument D19 at ILL.[50]

Each of the three VIVALDI samples was structurally characterized by neutron diffraction at both 120 and 4 K. The cobalt sample was also run at 288 K, as a representative sample to assess the room-temperature structure of the series. The cobalt sample adopts a completely ordered structure at 4 K in $P\bar{4}$, whereas the nickel and zinc samples still show some disorder as a consequence of varying cooling rates (vide supra). The cobalt sample remains ordered on warming to 120 K (albeit with some elongation of urea oxygen atom anisotropic displacement parameters), while the disorder in the zinc sample increases. All of the samples, however, show some ordering at low temperature as the occupancies are significantly removed from an exact 50:50 ratio. At room temperature, all three samples were essentially randomly disordered.

In the ordered structure of **1a** with the water tetramer fixed in position, the water square exerts a pronounced effect upon the geometry of the cavity in which it resides. The solvent water bridges between two carbonyl oxygen atoms and, in doing so, draws them closer to each other (Figure 7). The four carbonyl groups form a parallelogram shape, rather than the crystallographically averaged square in the disordered structures. The difference in distance between pairs of oxygen atoms is substantial at 0.843 Å. It is thought that this long-range ordering is brought about by the π-stacking between the individual $[M(L)_4(H_2O)_2]^{2+}$ units within a chain of complexes. When the ligands of one unit become "pinched", this conformation is

(47) Jeffrey, G. A. *An Introduction to Hydrogen Bonding*, 1st ed.; Oxford University Press: Oxford, 1997.
(48) Wilkinson, C.; Cowan, J. A.; Myles, D. A. A.; Cipriani, F.; McIntyre, G. J. *Neutron News* **2002**, *13*, 37−41.
(49) Cole, J. M.; McIntyre, G. J.; Lehmann, M. S.; Myles, D. A. A.; Wilkinson, C.; Howard, J. A. K. *Acta Crystallogr., Sect. A* **2001**, *57*, 429−434.
(50) Mason, S. A.; Forsyth, V. T.; Howard, J. A. K.; Davidson, M. G.; Fuller, W.; Myles, D. A. D19: A fast new diffractometer for chemical crystallography, small proteins and fibre diffraction. In *Opportunities for Neutron Scattering in the 3rd Millennium*; Dianoux, J., Ed.; Institue Laue-Langevin: Grenoble, 2001; pp 332−334.

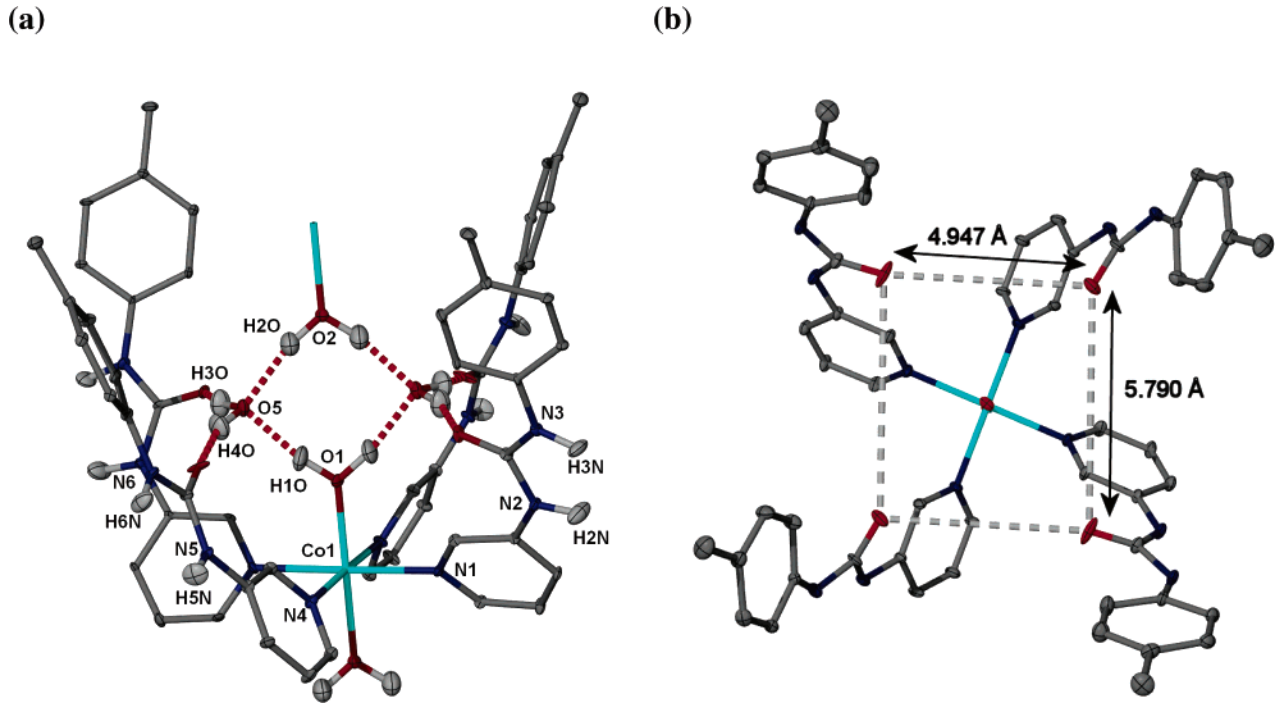

Figure 7. (a) Thermal ellipsoid plot (70%) showing hydrogen-bonding scheme for the ordered 4 K neutron structure of the Co complex **1a**, in $P\bar{4}$. (b) Cavity dimensions at 120 K; the sides of the cavity at which the water is bound show a significant contraction compared to the "empty" side.

Table 3. Hydrogen Bond Data for Interactions Involving the Water Molecules in the 4 K Structures of **1a**, **1b**, and **1d**[a]

	d(D—H)/Å	*d*(H···A)/Å	*d*(D···A)/Å	∠(D—H···A)/°
		Co Complex (**1a**)[a]		
O(1)—H(1O)···O(5)	0.972(5)	1.738(6)	2.699(3)	169.4(5)
O(2)—H(2O)···O(5)#1	0.967(6)	1.784(6)	2.737(4)	168.0(5)
O(5)—H(3O)···O(3)	0.971(6)	1.744(6)	2.679(4)	160.7(5)
O(5)—H(4O)···O(4)	0.956(6)	1.763(6)	2.686(4)	161.1(5)
		Ni Complex (**1b**)		
O(1)—H(1O)···O(5)	0.962(13)	1.738(14)	2.685(8)	167.9(12)
O(2)—H(2O)···O(5)#1	0.944(15)	1.825(16)	2.753(9)	166.9(13)
O(5)—H(3O)···O(3A)	0.990(18)	1.74(3)	2.68(3)	157.0(17)
O(5)—H(3O)···O(3B)	0.990(18)	2.21(4)	3.09(3)	147.7(15)
O(5)—H(4O)···O(3A)#2	1.002(16)	1.91(2)	2.782(17)	144.3(15)
O(5)—H(4O)···O(3B)#2	1.002(16)	1.721(18)	2.685(12)	160.3(18)
		Zn Complex (**1d**)		
O(1)—H(1O)···O(5)	0.977(8)	1.741(9)	2.711(5)	171.2(7)
O(2)—H(2O)···O(5)#3	0.974(8)	1.796(9)	2.759(5)	169.2(7)
O(5)—H(3O)···O(3A)	0.982(10)	1.935(14)	2.778(9)	142.4(9)
O(5)—H(3O)···O(3B)	0.982(10)	1.733(11)	2.675(8)	159.5(10)
O(5)—H(4O)···O(3A)#4	0.989(11)	1.737(18)	2.686(14)	159.3(10)
O(5)—H(4O)···O(3B)#4	0.989(11)	2.25(2)	3.140(18)	149.2(8)

[a] Fewer data due to ordered structure. Symmetry operators: #1, *x*,*y*,*z*+1; #2, *y*,−*x*+$^1/_2$,*z*; #3, *x*,*y*,*z*−1; #4, y,−*x*+$^3/_2$,*z*. O(1) = upper aqua ligand, O(2) = lower aqua ligand, O(5) = enclathrated water, O(3) and O(4) = carbonyl oxygen atoms.

passed along to the next unit in the chain, promoting the ordering of the water, and so on. Interactions between stacks are mediated by hydrogen bonding to sulfate.

The hydrogen bond data relating to the four water molecules in the 4 K neutron diffraction structures are shown in Table 3. The H···O(5) distances from the aqua ligands to the enclathrated water are marginally shorter from the aqua ligand with the longest M−O bond length, O(2), although the differences are similar to the experimental errors. Thus, it appears that there is a negligible difference in the hydrogen bonding of the two aqua ligands and the water square is relatively equidimensional. The requirements of hydrogen bonding within the water tetramer therefore dominate over the requirements of the M−OH_2 bonds.

PACHA Calculations. The coordinates of the ordered 120 K structure of **1a** were used as input into fixed geometry calculations using PACHA.[5] The PACHA method allows for the nonempirical quantification of van der Waals interactions and hydrogen bonds starting from a diffraction model (to give the relative spatial positions of the atoms) and two ab initio parameters for each element (the configuration energy and the radius of the most diffuse valence orbital), using the electrostatic energy of the system. This algorithm derives from the fact that the total energy of a system may always be split between a purely electrostatic contribution, the electrostatic balance, EB, and a purely electronic contribution, *F*. This is known as the ground-state Hellmann−Feynman decomposition, E_{TOT} = EB + *F*. The electrostatic contribution that is applied in PACHA

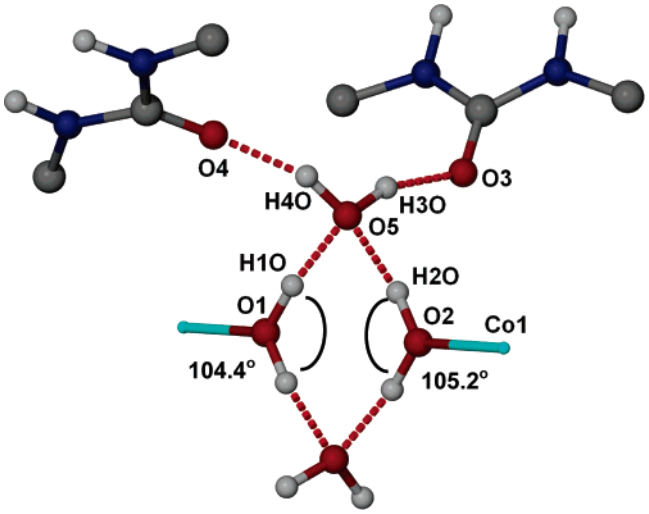

Figure 8. The four hydrogen bonds that surround each enclathrated water molecule (two received from the aqua ligands and two donated to urea carbonyl groups), with the atom labeling used for calculations. The initial PACHA calculations assume these interactions to be of equal strength.

is based solely upon classical interactions between fixed nuclei and moving electronic clouds using a spherical charge approximation. The structure is not allowed to relax in any way during the calculation, in order not to perturb the electronic contributions, F, and allowing us, therefore, to probe interaction energies from the sole knowledge of the EB contribution. In practical terms, the algorithm utilizes the fact that fragments of the structure can be separated, and providing that no geometrical change occurs, the situation in eq 1 may be approximated; i.e., the interaction between the two fragments has an energy related only to the total EB and the individual EB values of the fragments.

$$\Delta H \approx \mathrm{EB_{TOT}} - (\mathrm{EB_1} + \mathrm{EB_2}) \quad (1)$$

For the computational work, energies were derived using the unit cell contents rather than the molecular formula; therefore, the working model was $Co_2(L)_8(SO_4)_2(H_2O)_8$. Both of the enclathrated water molecules receive two hydrogen bonds (from the aqua ligands) and donate two hydrogen bonds (to urea carbonyl groups) (Figure 8). These hydrogen bonds (16 in total within the unit cell) were first assumed to be of equivalent strength, eq 2, where E_{HB} = average hydrogen bond energy.

$$E_{HB}(\mathrm{water}) = \Delta E(\mathrm{water})/16 \quad (2)$$

The value of ΔE(water) may be calculated by removing the enclathrated water molecules (i.e., the atoms O(5), H(3O), and H(4O)) from the model and working out the energy difference between the total system and the sum of the dehydrated framework and the individual free water molecules, eq 3.

$$\Delta E(\mathrm{water}) = \mathrm{EB}[Co_2(L)_8(SO_4)_2(H_2O)_8] - \mathrm{EB}[Co_2(L)_8(SO_4)_2(H_2O)_4] - 4\mathrm{EB}[H_2O] \quad (3)$$

The complete structure was calculated to have a value of $\mathrm{EB}[Co_2(L)_8(SO_4)_2(H_2O)_8] = -5530.2$ kJ mol^{-1}. When the enclathrated molecules are removed, the remaining system has a value $\mathrm{EB}[Co_2(L)_8(SO_4)_2(H_2O)_4] = -4363.1$ kJ mol^{-1}. The computed energy for an individual enclathrated water molecule was based upon the frozen solid-state conformation observed and found to be $\mathrm{EB}[H_2O] = -175.4$ kJ mol^{-1}. When these values are used in eqs 2 and 3, this leads to E_{HB}(water) $= -29.1$ kJ mol^{-1}. This energy value is approximately 26% stronger than that for the interactions within hexagonal ice.[5]

The water square was then investigated in more detail in terms of the aqua ligands. A suitable model could not be obtained by simply removing the aqua ligands from the structure, as this would not only disrupt hydrogen bonding but also break Co−O bonds. The approach used was to rotate the ligands around the Co−O axis, thus disrupting the hydrogen-bonding network but leaving all covalent bonds intact.

The aqua ligands were studied independently, and during their rotation both the EB and the change in steric repulsion were recorded (which ensures no relaxation of the structure occurs). The effects of rotating the "upper" aqua ligand through 360° (rotation of the Co(1)−O(1) bond) show that there is no change in the repulsive energy of the system, indicating that there is no steric congestion associated with the water square. The curve associated with the change in EB clearly shows that there are two highly favorable orientations for the aqua ligand to adopt at τ(H(1O)−O(1)−Co(1)−O(5)) = 0° and 180°. These values correspond to the observed positions of the two hydrogen atoms of the aqua ligand in the neutron structure. The amplitude of the line is $\Delta E = -70.2$ kJ mol^{-1}, which corresponds to the energy involved in breaking the four hydrogen bonds that the axial water donates to the enclathrated water (i.e., the H(1O)···O(5) interactions). The energy associated with a single H(3O)···O(5) interaction is therefore E_{HB}(O(1)) $= -17.6$ kJ mol^{-1}, which is a significantly lower value than that found for the average E_{HB}(water) (-29.1 kJ mol^{-1}). The same rotation was applied to the "lower" O(2) aqua ligand. As expected, two minima are clearly observed at the same torsion angles as for the Co(1)−O(1) bond rotation. However, the amplitude of the line is larger, $\Delta E = -81.0$ kJ mol^{-1}, meaning that the energy associated with one H(2O)···O(5) hydrogen bond is also significantly larger, E_{HB}(O(2)) $= -20.3$ kJ mol^{-1}.

Knowledge of the average value of the strength of hydrogen bonds in the structure, E_{HB}(water), as well as precise values for the interactions involving the aqua ligands, E_{HB}(O(1)) and E_{HB}(O(2)), allows for more accurate values to be obtained for the interactions between the enclathrated water and the urea carbonyl groups. This may be calculated by regarding separately the energy of the hydrogen bonds that form the square, E_{HB}(intra), and those that tether the square to the carbonyl groups, E_{HB}(inter). The total value of the hydrogen bonds within one square is given by

$$E_{HB}(\mathrm{intra}) = 2[\mathrm{E_{HB}(O1)} + E_{HB}(\mathrm{O2})] \quad (4)$$

and the total energy of the hydrogen bonds within the whole $Co_2(L)_8(SO_4)_2(H_2O)_8$ unit cell can be broken down into

$$\Delta E(\mathrm{water}) = 2E_{HB}(\mathrm{intra}) + 8E_{HB}(\mathrm{inter}) \quad (5)$$

It follows from eqs 4 and 5 that E_{HB}(inter) can be calculated as follows:

$$E_{HB}(\mathrm{inter}) = [\Delta E(\mathrm{water}) - 2E_{HB}(\mathrm{intra})]/8 \quad (6)$$

Substituting the values obtained into eq 6 results in a value of E_{HB}(inter) $= -39.3$ kJ mol^{-1}.

Table 4. Hydrogen Bond Data for the Ordered Cobalt Complex **1a** at 120 K alongside the Calculated Hydrogen Bond Strengths

	d(D—H)/Å	*d*(H···A)/Å	*d*(D···A)/Å	∠(D—H···A)/°	E_{HB}/ kJ mol^{-1}
O(1)—H(1O)···O(5)	0.960(7)	1.758(7)	2.707(4)	169.1(6)	−17.6
O(2)—H(2O)···O(5)	0.964(7)	1.798(7)	2.746(4)	167.1(6)	−20.3
O(5)—H(3O)···O(3)	0.993(7)	1.742(7)	2.696(5)	159.8(6)	−39.9
O(5)—H(4O)···O(4)	0.973(7)	1.750(7)	2.687(5)	160.6(6)	−39.9

The hydrogen bonds involving water in this structure span an energy range of 18−39 kJ mol^{-1}. Those involving the aqua ligands are weaker (−17.6 and −20.3 kJ mol^{-1}) than those involving the carbonyl groups (−39.3 kJ mol^{-1}). The comparisons between the calculated strengths of the hydrogen bonds and their geometric parameters are shown in Table 4. Initially these results appear contrary to expectations, as the shortest hydrogen bond to O(5) is not the strongest one. This phenomenon can, however, be explained by further examination of the water square.

The water tetramer can be studied as a discrete entity, removed from the confines of the cavity. This allows for the water tetramer to be studied without the steric constraints that are imposed on it within the solid-state structure. For the O(1)···O(5)···O(2)···O(5) water tetramer, it is found that EB[$(H_2O)_4$] = −800.3 kJ mol^{-1}. The O(1) water molecule may be removed, breaking two H(1O)···O(5) contacts and leaving an O(5)···O(2)···O(5) trimer. Using the EB values for the removed water and the remaining trimer, EB[O(1)] = −166.5 kJ mol^{-1} and EB[$(H_2O)_3$] = −583.5 kJ mol^{-1}, respectively, it follows that

$$E_{HB}(O1) = (EB[(H_2O)_4] - EB[O(3)] - EB[(H_2O)_3])/2 \quad (7)$$

Substituting the known values into eq 7 gives a value of E_{HB}(O1) = −25.2 kJ mol^{-1}. An analogous procedure was carried out for the O(2). The values of EB[O(2)] = −172.1 kJ mol^{-1} and EB[$(H_2O)_3$] = −572.8 kJ mol^{-1} were found, which gave E_{HB}(O2) = −27.7 kJ mol^{-1}.

These gas-phase values of E_{HB}(O1) and E_{HB}(O2), compared to those in Table 4, show that the inclusion of the water tetramer within the solid-state cavity acts to weaken the hydrogen bonds that hold the tetramer together, with a similar degree of weakening observed for both the O(1) and O(2) hydrogen bonds (ΔE = +7.6 and +7.4 kJ mol^{-1}, respectively).

In addition to examining the role played by the solid-state inclusion of the tetramer, we also studied the geometrical constraints arising from the confinement of the tetramer within the cavity. The enclathrated water, O(5), is positioned closer to O(1) than to O(2). There is therefore less electrostatic repulsion between the H(2O)···H(3O) and H(2O)···H(4O) pairs (2.39 and 2.45 Å, respectively) than there is between the H(1O)···H(3O) and H(1O)···H(4O) pairs (2.21 and 2.25 Å, respectively). The H−O−H angles within the aqua ligands are also different, with the angle at O(1) being smaller (104.7° compared to 105.6°). The smaller angle in the O(1) ligand results in increased H···H repulsion within the aqua ligand compared to that in the O(2) ligand. The lower repulsive forces between hydrogen atoms account for the higher stability of the O(5)···O(2)···O(5) trimer in the gas-phase calculations (by 10.7 kJ mol^{-1}) and for the fact that more electrostatic energy is stored in the H(2O)···O(5) bond.

The extra energy of the H(2O)···O(5) that these calculations reveal explains the distortion of the metal center. The stronger hydrogen bonding between ligand and solvent causes the lower aqua ligand to be pulled deeper into the cavity, resulting in the inequality of the M−O bond lengths.

The consideration of hydrogen···hydrogen repulsions explains why simply looking at the O—H···O distances cannot accurately account for differences in the strengths of hydrogen bonds. Although it is true for simple water dimers that shorter O···O distances give stronger hydrogen bonds, this fact only arises because the hydrogen atoms are free to adopt a geometry that minimizes repulsive interactions. The tetramer cluster, however, represents a dimer of dimers in which the hydrogen atoms are forced into closer proximity. It is for these reasons that water tetramers are rarely seen within solid-state structures, with water clusters preferring to adopt five- and six-membered rings instead, as exemplified by clathrate hydrates.[20]

Another interesting feature of the hydrogen bonding within these structures is the comparison between the hydrogen bonds involving the water molecules and the urea···sulfate interactions. The calculation of the sulfate interactions was conducted in an manner analogous to those involving the water, with the sulfate being removed from the structure (atoms S(1), S(2), O(6), and O(7)), breaking all of the NH···O hydrogen bonds (eq 8).

$$\Delta E(SO_4) = EB[Co_2(SO_4)_2(H_2O)_8(L)_8] - EB[Co_2(H_2O)_8(L)_8] - 2EB[SO_4] \quad (8)$$

The network with the sulfate anions removed was calculated to have EB[$Co_2(H_2O)_8(L)_8$] = −4599.9 kJ mol^{-1}, and the isolated anions, frozen in their solid-state geometry, were calculated to have EB[SO_4] = −224.3 kJ mol^{-1}. It follows from eq 8 that $E_{HB}(SO_4)$ = −481.7/16 = −30.1 kJ mol^{-1}. This value is close to the average value of the OH···O interactions (−29.1 kJ mol^{-1}), which is unusual. Most structures display significantly stronger interactions from OH donors than from NH groups, whereas within this structure there is an almost perfect energetic balance between the two.

Thermogravimetric Analysis. Microcrystalline samples of the cobalt, nickel, and zinc complexes (**1a**, **1b,** and **1d**) were all examined using TGA. Crystals of the copper complex (**1c**) could not be acquired in sufficient quantity to be suitable for analysis, so a bulk powder sample was used instead. The samples were studied over the temperature range 30−300 °C, using a heating rate of 10 °C min^{-1}. The TGA traces showed, in all cases, clear mass decreases corresponding to the loss of water from the sample; however, the onset temperature of the mass loss and the trace profiles obtained are different for the four different materials. The four complexes are of very similar molecular weights (the minor differences arising from the change in the metal center), and approximate percentage values for relevant mass losses are 1.6% for a water molecule and 20% for an L ligand. It can therefore be deduced that a 3.2% mass loss corresponds to two enclathrated water molecules being removed, and that a loss of around 6.4% accounts for all of the water molecules in the sample.

The TGA trace obtained for the nickel complex (**1b**) shows one clear mass loss step with an onset temperature around 130 °C, which corresponds to the loss of both the enclathrated and

coordinated water molecules within the sample. The loss is gradual, taking place over a range of about 60 °C, suggesting that there may be two overlapping processes that cannot be distinguished (i.e., the loss of enclathrated water closely followed by the aqua ligands). At 230 °C, decomposition of the sample begins, detectable by a rapid mass decrease. The powder sample of the copper complex also displays a single decrease, accounting for the loss of the four water molecules, although the onset temperature is significantly lower than that of the nickel complex, 82 °C, and the process occurs over a shorter temperature range. After the loss of the water molecules within the sample, the mass remains almost constant until decomposition begins at 210 °C. It is believed that the lower onset temperature of the water loss is due to the water being less tightly bound than that of the nickel complex due to the Jahn−Teller distortion of the copper(II) center. This may also account for the shorter temperature range over which the mass loss occurs.

The zinc complex displays behavior significantly different than that of the nickel and copper complexes. The loss of the four water molecules begins at just over 150 °C, immediately followed by a second, larger mass loss. This second process is attributed to the loss of one of the L ligands that begins while the water molecules are still leaving. At 213 °C, the percentage of the total weight that has been lost corresponds to that of all of the water molecules and one of the L ligands (ca. 26%). After this point, decomposition of the sample occurs.

The cobalt-containing material **1a** initially proved problematic to assess, as vastly differing traces were obtained from various samples, most displaying poorly reproducible weight loss in multiple, sharp steps. These anomalous results are attributed to crystal defects that contain pockets of water. The crystals obtained of $[Co(L)_4(H_2O)_2]SO_4 \cdot 2H_2O$ were significantly larger than those of the other three samples and, when viewed under a microscope, can be seen to contain small defects. When a sample was run without being powdered prior to the experiment, the crystals were observed to bubble briefly during the temperature increase. This is believed to correspond to water/steam trapped in the defects reaching sufficient pressure to break the crystal and rapidly evaporate. With powdered samples, only a single mass loss corresponding to all four water molecules and one ligand is observed before decomposition begins at 210 °C. Figure 9 shows the comparison of samples of the cobalt complex run as whole crystals and run as a powder. Similar effects were noted for large crystals of the Zn complex and are believed to be responsible for the sharp mass loss steps noted in the preliminary communication.[31]

The TGA experiments on the $[M(L)_4(H_2O)_2]SO_4 \cdot 2H_2O$ complexes confirm that there are two enclathrated water molecules *per* formula unit, as expected from diffraction and elemental analysis results. The experiments show that the enclathrated water molecules are strongly incorporated as part of the structures. In all cases, the mass losses corresponding to the enclathrated water and the aqua ligands are indistinguishable. Although it is likely that the enclathrated water is lost before the aqua ligands, the temperatures required for their removal are very similar and well above 100 °C (130−160 °C for Co, Ni, and Zn; 82 °C for Cu), suggesting that the hydrogen bonding that holds the structure together must be of a significant strength.

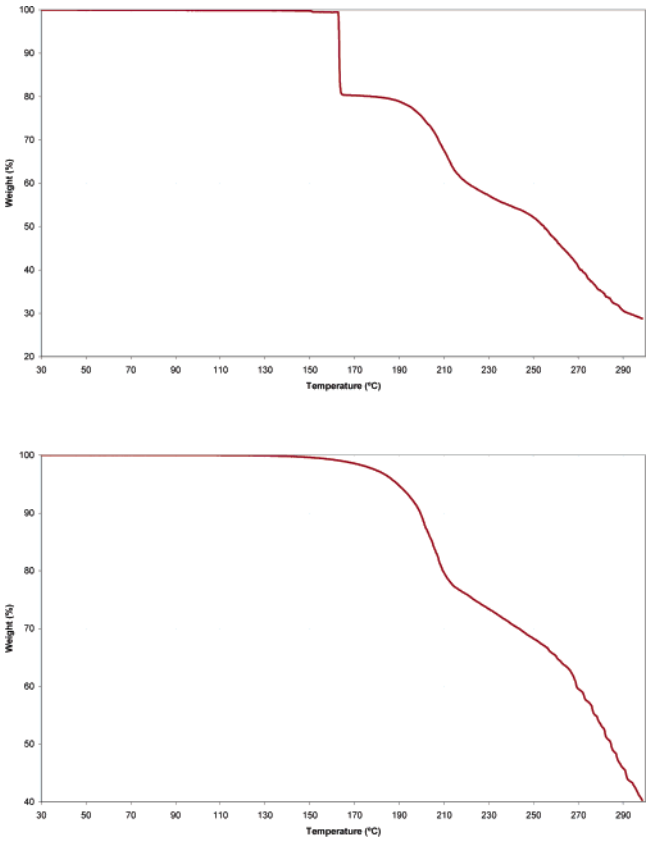

Figure 9. TGA traces of $[Co(L)_4(H_2O)_2]SO_4 \cdot 2H_2O$, showing the comparison between a crystalline sample (top) and a powdered sample (bottom). Apart from the sharp mass loss in the crystalline sample, caused by water trapped in a defect, the behavior of the samples is nearly identical.

Summary and Conclusion

The $[M(L)_4(H_2O)_2]SO_4 \cdot 2H_2O$ series of complexes displays interesting solid-state structures, containing a highly unusual water tetramer. These result from a high degree of hydrogen bonding, both within the cavities and between parallel chains via the sulfate counteranions.

The enclathrated water molecules significantly influence the structure. TGA experiments show that they are held within the structure almost as tightly as the coordinated water due to the extent of the hydrogen-bonding interactions in which they partake. Neutron diffraction data have provided high-precision, low-temperature structures of the cobalt complex, showing the ordering of the water tetramer that occurs as the sample is slowly cooled. The hydrogen bonding involving the solvent molecules plays a more pronounced role at low temperature, pulling together two sides of the $[M(L)_4(H_2O)_2]^{2+}$ complex. The apparent strength and integrity of the water square lends indirect and tacit support to the model proposed by Benson and Siebert.[22]

Nonempirical calculations have allowed for a detailed examination of the strengths of the interactions, showing that, on average, the OH···O interactions are stronger than those in ice. These calculations have also shown the effect that incarceration of the water tetramer within the cavity has on the strengths of the interactions compared to a free $(H_2O)_4$ unit. The repulsions within the enclosed environment result in interactions between the lower aqua ligand and the enclathrated water molecule being stronger than those with the upper ligand. This energy difference manifests itself as a distortion of the octahedral coordination

sphere of the metal center. The calculations also highlight the breakdown of the hydrogen bond strength−length analogy[51−54] in constrained solid-state lattices, particularly in cyclic cases.

Experimental Section

Materials and Methods. All purchased materials were of commercial quality and were used without further purification. Reactions were carried out under air, and no air sensitivity was observed for any of the products obtained. Microanalyses for C, H, and N were recorded at either the University of Durham or the University of North London. TGA experiments were conducted at the University of Durham using a Pyris 1 instrument. Ligand L was prepared as previously described.[35] Conditions were optimized for the growth of diffraction-quality crystals, which were kept immersed in mother liquor until used. As a result, yields were not measured but are estimated to be essentially quantitative from the lack of residual color in the mother liquor.

$[Co(L)_4(H_2O)_2]SO_4\cdot 2H_2O$, 1a. Crystals were grown from a solution of L (0.025 g, 0.11 mmol) and $CoSO_4\cdot 7H_2O$ (0.010 g, 0.04 mmol) in a water/methanol solution (50:50 v/v) (5 mL) at room temperature. Anal. Calcd for $C_{52}H_{60}N_{12}O_{12}CoS$: C, 54.97; H, 5.32; N, 14.79. Found: C, 55.08; H, 5.33; N, 14.93.

$[Ni(L)_4(H_2O)_2]SO_4\cdot 2H_2O$, 1b. Crystals were grown from a solution of L (0.025 g, 0.11 mmol) and $NiSO_4\cdot 6H_2O$ (0.010 g, 0.04 mmol) in a water/methanol solution (50:50 v/v) (5 mL) at room temperature. Anal. Calcd for $C_{52}H_{60}N_{12}O_{12}NiS$: C, 54.99; H, 5.32; N, 14.80. Found: C, 55.10; H, 5.34; N, 14.87.

$[Cu(L)_4(H_2O)_2]SO_4\cdot 2H_2O$, 1c. Crystals were grown from a solution of L (0.025 g, 0.11 mmol) and $CuSO_4\cdot 5H_2O$ (0.009 g, 0.04 mmol) in a water/methanol solution (50:50 v/v) (5 mL) at room temperature. Anal. Calcd for $C_{52}H_{60}N_{12}O_{12}CuS$: C, 54.75; H, 5.30; N, 14.73. Found: C, 54.78; H, 5.37; N, 14.80%.

$[Zn(L)_4(H_2O)_2]SO_4\cdot 2H_2O$, 1d. Crystals were grown from a solution of L (0.025 g, 0.11 mmol) and $ZnSO_4\cdot 7H_2O$ (0.011 g, 0.04 mmol) in a water/methanol solution (50:50 v/v) (5 mL) at room temperature. Anal. Calcd for $C_{52}H_{60}N_{12}O_{12}ZnS$: C, 54.66; H, 5.29; N, 14.71. Found: C, 54.43; H, 5.25; N, 14.60.

Large crystals for neutron diffraction experiments were grown by gradual addition over a period of weeks of aliquots of metal salt and ligand L to a 1-L flask of methanol/water (50:50 v/v) at room temperature.

X-ray Crystallography. Suitable single crystals were mounted using silicon grease on a thin glass fiber. Crystallographic measurements were carried out using either a Nonius KappaCCD or a Bruker SMART 1000. Both instruments were equipped with graphite monochromatic Mo Kα radiation ($\lambda = 0.71073$ Å). The standard data collection temperature was 120 K, maintained using an open-flow N_2 Oxford Cryostream device. Integration was carried out using the Denzo-SMN[55] package. Data sets were corrected for Lorentz and polarization effects and for the effects of absorption. Structures were solved using direct methods in SHELXS-97[56] and developed using conventional alternating cycles of least-squares refinement with SHELXL-97[57] and difference Fourier synthesis with the aid of the graphical interface program XSeed.[58] In all cases, non-hydrogen atoms were refined anisotropically. C−H hydrogen atoms were fixed in idealized positions and allowed to ride on the atom to which they were attached. Hydrogen atom thermal parameters were tied to those of the atom to which they were attached. O−H and N−H hydrogen atoms were located experimentally and their positional and displacement parameters refined. All calculations were carried out on an IBM-compatible personal computer. Molecular graphics were produced using the program POV-Ray.[59]

Crystal data for $[Co(L)_4(H_2O)_2]SO_4\cdot 2H_2O$, **1a**, at 120 K: $C_{52}H_{60}N_{12}CoO_{12}S$, $M = 1136.11$, red block, $0.20 \times 0.12 \times 0.08$ mm^3, tetragonal, space group $P4/n$ (No. 85), $a = b = 18.070(3)$ Å, $c = 8.0756(16)$ Å, $V = 2636.9(7)$ Å^3, $Z = 2$, $D_c = 1.431$ g/cm^3, $F_{000} = 1190$, Nonius KappaCCD, Mo Kα radiation, $\lambda = 0.71073$ Å, $T = 120(2)$ K, $2\theta_{max} = 55.0°$, 4640 reflections collected, 3006 unique ($R_{int} = 0.0345$), $R1 = 0.0419$, $wR2 = 0.0977$, R indices based on 2863 reflections with $I > 2\sigma(I)$ (refinement on F^2), 218 parameters, 0 restraints. Lp and absorption corrections applied, $\mu = 0.440$ mm^{-1}.

Crystal data for $[Co(L)_4(H_2O)_2]SO_4\cdot 2H_2O$, **1a**, slow-cooled to 30 K: $C_{52}H_{60}CoN_{12}O_{12}S$, $M = 1136.11$, orange block, $0.30 \times 0.25 \times 0.20$ mm^3, tetragonal, space group $P\bar{4}$ (No. 81), $a = b = 18.084(3)$ Å, $c = 8.054(2)$ Å, $V = 2633.9(9)$ Å^3, $Z = 2$, $D_c = 1.433$ g/cm^3, $F_{000} = 1190$, Bruker SMART-1K CCD diffractometer, Mo Kα radiation, $\lambda = 0.71073$ Å, $T = 30(2)$ K, $2\theta_{max} = 55.0°$, 12 375 reflections collected, 5805 unique ($R_{int} = 0.0304$), final goodness-of-fit = 1.025, $R1 = 0.0304$, $wR2 = 0.0785$, R indices based on 5340 reflections with $I > 2\sigma(I)$ (refinement on F^2), 388 parameters, 0 restraints. Lp and absorption corrections applied, $\mu = 0.441$ mm^{-1}. Absolute structure parameter = 0.599(11) (racemic twin model applied).

Crystal data for $[Ni(L)_4(H_2O)_2]SO_4\cdot 2H_2O$, **1b**: $C_{52}H_{60}N_{12}NiO_{12}S$, $M = 1135.89$, blue block, $0.18 \times 0.10 \times 0.08$ mm^3, tetragonal, space group $P4/n$ (No. 85), $a = b = 18.028(3)$ Å, $c = 8.1143(16)$ Å, $V = 2637.3(7)$ Å^3, $Z = 2$, $D_c = 1.430$ g/cm^3, $F_{000} = 1192$, Nonius KappaCCD, Mo Kα radiation, $\lambda = 0.71073$ Å, $T = 120(2)$ K, $2\theta_{max} = 54.9°$, 4145 reflections collected, 2549 unique ($R_{int} = 0.0564$), $R1 = 0.0396$, $wR2 = 0.0807$, R indices based on 1747 reflections with $I > 2\sigma(I)$ (refinement on F^2), 218 parameters, 0 restraints. Lp and absorption corrections applied, $\mu = 0.483$ mm^{-1}.

Crystal data for $[Cu(L)_4(H_2O)_2]SO_4\cdot 2H_2O$, **1c**: $C_{52}H_{60}N_{12}CuO_{12}S$, $M = 1140.72$, blue plate, $0.10 \times 0.10 \times 0.05$ mm^3, tetragonal, space group $P4/n$ (No. 85), $a = b = 17.846(3)$ Å, $c = 8.3019(17)$ Å, $V = 2644.0(8)$ Å^3, $Z = 2$, $D_c = 1.433$ g/cm^3, $F_{000} = 1194$, Nonius KappaCCD, Mo Kα radiation, $\lambda = 0.71073$ Å, $T = 120(2)$ K, $2\theta_{max} = 54.9°$, 4681 reflections collected, 3021 unique ($R_{int} = 0.0344$), $R1 = 0.0397$, $wR2 = 0.0881$, R indices based on 2499 reflections with $I > 2\sigma(I)$ (refinement on F^2), 215 parameters, 0 restraints. Lp and absorption corrections applied, $\mu = 0.527$ mm^{-1}.

Crystal data for $[Zn(L)_4(H_2O)_2]SO_4\cdot 2H_2O$, **1d**: $C_{52}H_{60}N_{12}ZnO_{12}S$, $M = 1142.55$, colorless block, $0.20 \times 0.20 \times 0.15$ mm^3, tetragonal, space group $P4/n$ (No. 85), $a = b = 18.0760(5)$ Å, $c = 8.1208(3)$ Å, $V = 2653.41(14)$ Å^3, $Z = 2$, $D_c = 1.430$ g/cm^3, $F_{000} = 1196$, Nonius KappaCCD, Mo Kα radiation, $\lambda = 0.71073$ Å, $T = 120(2)$ K, $2\theta_{max} = 54.9°$, 4854 reflections collected, 3031 unique ($R_{int} = 0.0428$), $R1 = 0.0397$, $wR2 = 0.0768$, R indices based on 2057 reflections with $I > 2\sigma(I)$ (refinement on F^2), 218 parameters, 0 restraints. Lp and absorption corrections applied, $\mu = 0.577$ mm^{-1}.

Neutron Crystallography. Neutron diffraction experiments were conducted at the Institut Laue-Langevin, Grenoble, using the VIVALDI Laue diffractometer with a white neutron beam (~0.8−5.0 Å). Samples were wrapped in aluminum foil and mounted on aluminum pins using epoxy resin. Laue diffraction patterns were collected at 4, 120, or 290 K, five to eight patterns at 20° intervals in rotation about an axis perpendicular to the beam in each set, with times for data collection ranging from 6 to 12 h for a full data set. The samples were cooled in a He flow cryostat. Data were indexed, integrated, and normalized to a common wavelength using the program Lauegen[60] and personal programs of Prof. Clive Wilkinson. No correction for absorption was judged necessary. Data were refined using conventional alternating least-

(51) Braga, D.; D'Oria, E.; Grepioni, F.; Mota, F.; Novoa, J. J.; Rovira, C. *Chem.-Eur. J.* **2002**, *8*, 1173−1180.
(52) Braga, D.; Grepioni, F.; Novoa, J. J. *Chem. Commun.* **1998**, 1959−1960.
(53) Mascal, M.; Marjo, C. E.; Blake, A. J. *Chem. Commun* **2000**, 1591−1592.
(54) Steiner, T. *Chem. Commun* **1999**, 2299−2300.
(55) Otwinowski, Z.; Minor, W. In *Methods in Enzymology*; Carter, C. W., Sweet, R. M., Eds.; Academic Press: London, 1997; Vol. 276, pp 307−326.
(56) Sheldrick, G. M. *SHELXS-97*; University of Göttingen: Göttingen, 1997.
(57) Sheldrick, G. M. *SHELXL-97*; University of Göttingen: Göttingen, 1997.
(58) Barbour, L. J. *J. Supramol. Chem.* **2001**, *1*, 189−191.
(59) Cason, C. J. *POV-Ray*, 3.5; Persistence of Vision Raytracer Pty Ltd.: http://www.povray.org/, 2002.
(60) Campbell, J. W.; Hao, Q.; Harding, M. M.; Nguti, N. D.; Wilkinson, C. *J. Appl. Crystallogr.* **1998**, *31*, 496−502.

squares cycles using SHELXL-97, starting from existing X-ray models, and Fourier maps were viewed using the program XSeed.[58] All atoms, including hydrogen, were treated anisotropically and allowed to refine freely. Cell parameters were determined from X-ray data with linear extrapolation to 4 K.

Crystal data for **1a** at 4 K in $P\bar{4}$: $C_{52}H_{60}CoN_{12}O_{12}S$, $M = 1135.00$, red block, 2.5 × 0.9 × 0.65 mm^3, tetragonal, space group $P\bar{4}$ (No. 81), $a = b = 18.000(3)$ Å, $c = 8.0441(16)$ Å, $V = 2636.9(7)$ Å^3, $Z = 2$, $D_c = 1.429$ g/cm^3, $F_{000} = 617$, VIVALDI, neutron radiation, $\lambda = 0.8-5.0$ Å, $T = 4(2)$ K, $2\theta_{max} = 142.2°$, 16 696 reflections collected, 7153 unique ($R_{int} = 0.1749$), $R1 = 0.0596$, $wR2 = 0.1052$, R indices based on 4783 reflections with $I > 2\sigma(I)$ (refinement on F^2), 621 parameters, 0 restraints. Lorentz corrections applied. Absolute structure parameter = 0(10).[61] Atom Co(1) was refined isotropically.

Crystal data for **1a** at 120 K in $P\bar{4}$: $C_{52}H_{60}CoN_{12}O_{12}S$, $M = 1135.00$, red block, 2.5 × 0.9 × 0.65 mm^3, tetragonal, space group $P\bar{4}$ (No. 81), $a = b = 18.070(3)$ Å, $c = 8.0756(16)$ Å, $V = 2636.9(7)$ Å^3, $Z = 2$, $D_c = 1.429$ g/cm^3, $F_{000} = 617$, VIVALDI, neutron radiation, $\lambda = 0.8-5.0$ Å, $T = 120(2)$ K, $2\theta_{max} = 142.6°$, 14 176 reflections collected, 5744 unique ($R_{int} = 0.1731$), $R1 = 0.0572$, $wR2 = 0.1053$, R indices based on 3733 reflections with $I > 2\sigma(I)$ (refinement on F^2), 622 parameters, 0 restraints. Lorentz corrections applied. Absolute structure parameter = 0(10).[61] Atoms S(1) and S(2) were refined isotropically.

Crystal data for **1a** at 288 K in $P4/n$: $C_{52}H_{60}CoN_{12}O_{12}S$, $M = 1135.00$, red block, 2.5 × 0.9 × 0.65 mm^3, tetragonal, space group $P4/n$ (No. 85), $a = b = 18.188(3)$ Å, $c = 8.1281(16)$ Å, $V = 2688.7(8)$ Å^3, $Z = 2$, $D_c = 1.402$ g/cm^3, $F_{000} = 617$, VIVALDI, neutron radiation, $\lambda = 0.8-5.0$ Å, $T = 288(2)$ K, $2\theta_{max} = 140.7°$, 18 558 reflections collected, 1823 unique ($R_{int} = 0.1360$), $R1 = 0.0406$, $wR2 = 0.0982$, R indices based on 1403 reflections with $I > 2\sigma(I)$ (refinement on F^2), 347 parameters, 0 restraints. Lorentz corrections applied.

Crystal data for **1b** at 4 K in $P4/n$: $C_{52}H_{60}N_{12}NiO_{12}S$, $M = 1134.00$, blue needle, 2.0 × 0.7 × 0.7 mm^3, tetragonal, space group $P4/n$ (No. 85), $a = b = 17.958(3)$ Å, $c = 8.0826(16)$ Å, $V = 2636.9(7)$ Å^3, $Z = 2$, $D_c = 1.428$ g/cm^3, $F_{000} = 633$, VIVALDI, neutron radiation, $\lambda = 0.8-5.0$ Å, $T = 4(2)$ K, $2\theta_{max} = 143.4°$, 13 451 reflections collected, 3325 unique ($R_{int} = 0.3636$), $R1 = 0.0999$, $wR2 = 0.2130$, R indices based on 1786 reflections with $I > 2\sigma(I)$ (refinement on F^2), 336 parameters, 6 restraints. Lorentz corrections applied. An ISOR restraint was placed on atom O(1A).

Crystal data for **1b** at 120 K in $P4/n$: $C_{52}H_{60}N_{12}NiO_{12}S$, $M = 1134.00$, blue needle, 2.0 × 0.7 × 0.7 mm^3, tetragonal, space group $P4/n$ (No. 85), $a = b = 18.028(3)$ Å, $c = 8.1143(16)$ Å, $V = 2637.2(7)$ Å^3, $Z = 2$, $D_c = 1.428$ g/cm^3, $F_{000} = 633$, VIVALDI, neutron radiation, $\lambda = 0.8-5.0$ Å, $T = 120(2)$ K, $2\theta_{max} = 141.2°$, 10 246 reflections collected, 1994 unique ($R_{int} = 0.2240$), $R1 = 0.0852$, $wR2 = 0.1958$, R indices based on 1341 reflections with $I > 2\sigma(I)$ (refinement on F^2), 332 parameters, 0 restraints. Lorentz corrections applied. The atom O(1A) was refined isotropically.

Crystal data for **1d** at 4 K in $P4/n$: $C_{52}H_{60}N_{12}O_{12}SZn$, $M = 1136.00$, colorless block, 1.75 × 1.2 × 1.2 mm^3, tetragonal, space group $P4/n$ (No. 85), $a = b = 18.0055(5)$ Å, $c = 8.0891(3)$ Å, $V = 2622.47(14)$ Å^3, $Z = 2$, $D_c = 1.439$ g/cm^3, $F_{000} = 623$, VIVALDI, neutron radiation, $\lambda = 0.8-5.0$ Å, $T = 4(2)$ K, $2\theta_{max} = 143.6°$, 18 825 reflections collected, 4162 unique ($R_{int} = 0.3030$), $R1 = 0.0623$, $wR2 = 0.1067$, R indices based on 2090 reflections with $I > 2\sigma(I)$ (refinement on F^2), 347 parameters, 0 restraints. Lorentz corrections applied.

Crystal data for **1d** at 120 K in $P4/n$: $C_{52}H_{60}N_{12}O_{12}SZn$, $M = 1136.00$, colorless block, 1.75 × 1.2 × 1.2 mm^3, tetragonal, space group $P4/n$ (No. 85), $a = b = 18.0760(5)$ Å, $c = 8.1208(3)$ Å, $V = 2653.41(14)$ Å^3, $Z = 2$, $D_c = 1.422$ g/cm^3, $F_{000} = 623$, VIVALDI, neutron radiation, $\lambda = 0.8-5.0$ Å, $T = 120(2)$ K, $2\theta_{max} = 141.8°$, 18 385 reflections collected, 2672 unique ($R_{int} = 0.2397$), $R1 = 0.0513$, $wR2 = 0.1191$, R indices based on 1616 reflections with $I > 2\sigma(I)$ (refinement on F^2), 347 parameters, 0 restraints. Lorentz corrections applied.

Crystal data for **1d** at 296 K in $P4/n$: $C_{52}H_{60}N_{12}O_{12}SZn$, $M = 1140.00$, colorless block, 1.75 × 1.2 × 1.2 mm^3, tetragonal, space group $P4/n$ (No. 85), $a = b = 18.1240(6)$ Å, $c = 8.1865(3)$ Å, $V = 2689.10(16)$ Å^3, $Z = 2$, $D_c = 1.408$ g/cm^3, $F_{000} = 623$, ILL D19, neutron radiation, $\lambda = 1.3160(2)$ Å, $T = 296(2)$ K, $2\theta_{max} = 120.4°$, 12 427 reflections collected, 3060 unique ($R_{int} = 0.0384$), $R1 = 0.0323$, $wR2 = 0.0580$, R indices based on 2427 reflections with $I > 2\sigma(I)$ (refinement on F^2), 374 parameters, 0 restraints. Lorentz and absorption corrections applied.

Acknowledgment. We thank the EPSRC for a studentship (to D.R.T.), ILL for beam time, and the Royal Society for provision of a microscope facility. J.W.S. thanks the Université Louis Pasteur for a visiting Professorship.

Supporting Information Available: Details of the X-ray and neutron crystal structures of **1a**−**d** at all temperatures (CIF). This material is available free of charge via the Internet at http://pubs.acs.org.

JA052081A

(61) Flack, H. D. *Acta Crystallogr., Sect. A* **1983**, *39*, 876−881.